APL Electronic Devices

RESEARCH ARTICLE | NOVEMBER 17 2025

Enhancing the contact performance of transition metal dichalcogenide-based field effect transistors using UV-induced doping

Somaditya Santra ; Sankalp Samdariya ; Shaili Sett ; Kenji Watanabe ; Takashi Taniguchi ; Arindam Ghosh

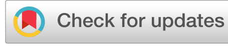

APL Electronic Devices 1, 046119 (2025)
https://doi.org/10.1063/5.0292130

View Online
Export Citation

Articles You May Be Interested In

Two-scale structure of the current layer controlled by meandering motion during steady-state collisionless driven reconnection

Phys. Plasmas (July 2004)

Single particle motion near an X point and separatrix

Phys. Plasmas (June 2004)

18 November 2025 09:30:49

APL Electronic Devices ARTICLE pubs.aip.org/aip/aed

Enhancing the contact performance of transition metal dichalcogenide-based field effect transistors using UV-induced doping

Cite as: APL Electron. Devices 1, 046119 (2025); doi: 10.1063/5.0292130
Submitted: 21 July 2025 • Accepted: 16 October 2025 •
Published Online: 17 November 2025

View Online

Export Citation

CrossMark

Somaditya Santra,[1] Sankalp Samdariya,[1] Shaili Sett,[1] Kenji Watanabe,[2] Takashi Taniguchi,[3] and Arindam Ghosh[1,4,a)]

AFFILIATIONS

[1] Department of Physics, Indian Institute of Science, Bangalore 560012, India
[2] Research Center for Electronic and Optical Materials, National Institute for Materials Science, 1-1 Namiki, Tsukuba 305-0044, Japan
[3] Research Center for Materials Nanoarchitectonics, National Institute for Materials Science, 1-1 Namiki, Tsukuba 305-0044, Japan
[4] Centre for Nanoscience and Engineering, Indian Institute of Science, Bangalore 560012, India

[a)] **Author to whom correspondence should be addressed:** arindam@iisc.ac.in

ABSTRACT

A persistent challenge in transition metal dichalcogenide (TMD)-based transistors is the formation of a Schottky Barrier (SB) at the metal–TMD interface which introduces substantial contact resistance and degrades device performance. Minimizing the barrier height and hence contact resistance—ideally to near-zero—is essential for realizing high-performance two dimensional (2D) material-based field-effect transistors. Here, we present a non-invasive photodoping strategy that leverages ultraviolet irradiation to induce localized n-type doping near the contact region, in hBN/TMD field-effect transistors. This targeted doping with UV exposure significantly reduces the SB, leading to a remarkable improvement in device performance. We demonstrate this with hBN/MoS_2 transistors, where we achieve a barrier height reduction of ~100 meV, resulting in a seventy-fold increase in on-state current and a twenty-fold increase in mobility. We further demonstrate the generality of this approach by applying it to other TMD transistors, such as hBN/$MoSe_2$ and hBN/WSe_2 hybrids, all of which exhibit similar performance enhancements. These results outline a portable, broadly applicable, and scalable contact engineering strategy for next-generation 2D electronic devices.

© 2025 Author(s). All article content, except where otherwise noted, is licensed under a Creative Commons Attribution-NonCommercial-NoDerivs 4.0 International (CC BY-NC-ND) license (https://creativecommons.org/licenses/by-nc-nd/4.0/). https://doi.org/10.1063/5.0292130

18 November 2025 09:30:49

I. INTRODUCTION

Two dimensional (2D) semiconductors are ideal for transistors due to their atomically thin channels, enabling excellent electrostatic control and aggressive scaling without short-channel effects beyond Si. Their lack of dangling bonds at the surface leads to clean, defect-free interfaces with dielectrics and minimizes surface scattering. However, large contact resistance due to a Schottky barrier (SB) at the metal–semiconductor (MS) interface remains a critical bottleneck, hindering efficient carrier injection and limiting device performance.[1,2] The SB at the MS junction primarily arises from the mismatch between the metal's work function and the semiconductor's electron affinity.[3–6] One widely used strategy to reduce the SB is by doping, which shifts the Fermi level upward (*n*-type) or downward (*p*-type), thereby aligning it with the Fermi level of the metal.[7] However, Fermi level pinning (FLP), which usually occurs at the MS interface due to metal-induced gap states, can make doping largely ineffective.[8,9]

Several approaches have been proposed to mitigate FLP and reduce contact resistance at the MS interface:

1. *Material pair engineering*: Selecting metal–transition metal dichalcogenide (TMD) combinations that exhibit favorable band alignment to minimize the SB.[10–13]
2. *Interface engineering*: FLP at the metal–MoS_2 interface can be reduced by using a low work-function material, such

as Indium. This strategy effectively de-pins the Fermi level and aligns it closer to the conduction band edge, enabling near-Ohmic contact behavior in monolayer MoS_2.[3]

3. *Interface layer insertion*: Incorporating an insulating or semiconducting layer between the metal and TMD to reduce electronic coupling and hence reduce the FLP effects.[14]
4. *Heavy doping*: Introducing high dopant concentrations near the contact region to modulate the band structure.[15,16] Localized chemical treatment of butyl lithium solution at the contact region of MoS_2 bilayers show a reduced contact resistance, due to the formation of a phase-transformed 1*T* metallic phase of MoS_2 that effectively behaves as the contact electrode.[17]

Each of these methods, however, present significant trade-offs. Bi has a relatively low work function of 4.26–4.3 eV, while Sb with a work function between 4.3 and 4.6 eV, depending on the crystal orientation.[10] This aligns well with the conduction band of monolayer MoS_2, and do not pin the Fermi level of MoS_2. However, these are very specific, limited solutions dependent on various parameters, such as the lattice orientation and thickness of MoS_2 layer. Interface layers may reduce pinning but often increase contact resistance. Substitutional doping can unintentionally affect the channel and damage the delicate TMD lattice, creating additional defects, such as sulfur vacancies.[18]

Photodoping presents a promising alternative offering a non-invasive procedure without the need for chemical or structural modification. As a physical process, it poses minimal risk of damaging the TMD lattice and may offer spatial control over doping profiles. Photo-induced doping has been previously demonstrated in hBN–graphene and hBN–TMD heterostructures, enabling stable, tunable, and even reversible doping effects. For example, Ju *et al.*[19] demonstrated gate-tunable photodoping in hBN–graphene under ultraviolet (UV) illumination. Khan *et al.*[20] showed localized photodoping in $MoTe_2$ using deep UV exposure with a gate bias, leveraging donor-like defect states in hBN to convert the *p*-type $MoTe_2$ to *n*-type. This doping was stable for over two weeks and enabled the formation of high-quality $p-n$ junctions. Photodoping was achieved in $MoSe_2$ encapsulated with hBN using a 785 nm laser.[21] The doping efficiency was strongly dependent on the resonant photoexcitation at the A-exciton peak, suggesting that absorption occurred primarily in the TMD layer rather than in hBN. In WSe_2/hBN heterostructures, reversible photodoping under low-intensity visible light has been demonstrated,[22] with doping effects that could be optically erased as well. Gadelha *et al.*[23] showed that MoS_2 on a Si/SiO_2 substrate could be *n*-doped by laser illumination at various wavelengths, with doping persisting in 77% of cases as measured by photocurrent suppression. UV doping can lead to long lasting *n*-type doping, especially under high vacuum conditions, provided there is a dielectric preventing the recombination of charges, as has been shown previously by Zhang *et al.*[24] in a Au/oxide/MoS_2 system.

18 November 2025 09:30:49

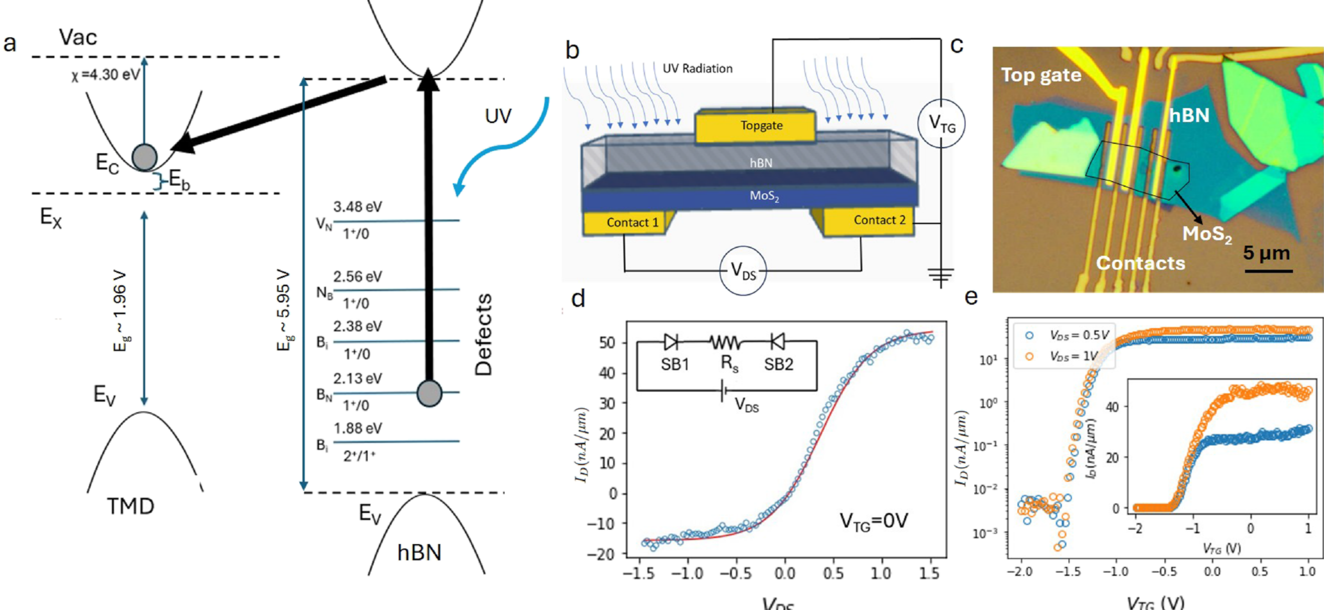

FIG. 1. Experimental strategy and initial characterization. (a) Schematic showing the UV-induced doping process in the hBN/TMD heterostructure, where E_X = excitonic energy level of the TMD, E_c and E_υ are the conduction band maxima and valence band minima, respectively, E_g is the bandgap, E_b is the binding energy of excitons in the TMD, and χ is the electron affinity of the TMD. (b) Proposed device schematic, with bottom-contacted metal electrodes on TMD and an hBN top layer, while the channel has a local top gate electrode. (c) Optical image of a typical device with MoS_2 as the TMD layer demarcated by a black boundary and hBN of thickness ≈20 nm on top. (d) Current–voltage characteristics in the pristine condition (circle), while the line is the fit to the experimental data. The inset of (d) shows the back-to-back Schottky diode model used to fit the experimental curve. (e) Transfer characteristics of the MoS_2 FET in semi-log scale at two different values of V_{DS}. The inset shows the same in linear scale.

© Author(s) 2025

Previous studies of photo-induced doping in 2D semiconductors predominantly focused on channel-targeted doping. In this work, we demonstrate a non-invasive UV-induced localized *n*-type photodoping strategy for hBN–TMD field-effect transistors (FETs), targeting only the MS contact regions. We propose that, under UV illumination, the valence electrons, particularly those near the hBN valence band (E_v), are optically excited to the conduction band (E_c). These electrons subsequently tunnel into the conduction band of the adjacent 2D semiconductor layer, which lies at a lower energy level [see schematic of Fig. 1(a)]. Since the semiconductor layer is electrically grounded, these electrons quickly dissipate, leaving behind locally positively charged sites in the hBN layer. This net positive charge exerts an electrostatic influence on the semiconductor layer lying in van der Waals proximity, inducing a corresponding negative charge density. As a result, the semiconductor layer experiences localized *n*-type doping, effectively shifting its Fermi level upward. Hence, the energy mismatch between the Fermi level of metal and semiconductor, for example, Au–MoS_2 junction, is reduced. This lowers the Schottky barrier at the MS junction, resulting in decreased contact resistance and improved carrier injection efficiency. Hence, using the UV-induced *n*-type doping, various FET parameters, such as mobility, ON–OFF ratio, and subthreshold swing, are improved.

We examine this hypothesis with a hBN/MoS_2 heterostructure in a field-effect device configuration with bottom-contacted Au source–drain electrodes and a local top gate, deposited only over the channel region as shown in the schematic of Fig. 1(b). Thus, even though the device is globally illuminated by UV, the top metal gate shields the channel region from exposure and preserves its intrinsic properties. We observe that the SB reduces by up to 100 meV, leading to significantly improved device performance, such as an increase in the ON-current by ≈seventy times along with substantial improvements in other FET device parameters. We also demonstrate that the UV-induced photodoping strategy to lower the SB at the MS junction is broadly applicable and compatible with other TMDs, such as WSe_2 and $MoSe_2$.

II. EXPERIMENT

A. Device fabrication

2D flakes of TMD and hBN were mechanically exfoliated onto standard SiO_2 (285 nm)/Si^{++}, allowing for optimal optical contrast during flake identification. The 2D heterostructure consisting MoS_2/hBN were picked up using a polycarbonate film on a PDMS stamp via a dry transfer method and placed on pre-patterned Cr/Au electrodes on SiO_2/Si^{++} substrates, with *a prior* O_2-plasma treatment. We ensure that Cr/Au has a thickness of (≈2 nm/5 nm) with metallization performed in high vacuum conditions, to minimize mechanical strain on the TMD layer and have a high-quality metal layer.[25] Thereafter, top gates were patterned by electron beam lithography, followed by metal deposition of Cr/Au (5 nm/50 nm) and lift off (supplementary material Sec. S1). The channel, which is the region covered by the top gate, has a length of ~1 μm of the 1.2 μm gap between the contacts. Figure 1(c) shows the optical image of the device post-fabrication. In this example, we show a bilayer MoS_2 with a top hBN (thickness ≈20 nm) encapsulation.

B. Irradiation methodology

A consistent UV doping procedure was applied to all heterostructure devices (hBN/MoS_2, hBN/WSe_2, and hBN/$MoSe_2$). Each device was sequentially exposed to progressively shorter UV wavelengths (λ) = 405, 365, 275, and 265 nm, beginning with the longest. The irradiation was done in pulses of 5, 10, or 20 s starting with the smallest. At each wavelength, the ON-state current was monitored until it reached saturation, after which the next shorter wavelength was applied. The time required for saturation depended on the LED power but was typically under 1000 s.

Electrical measurements were performed in a vacuum system with an optical window of quartz to allow UV light to enter. We used a source-meter for sending and measuring electrical signals, and also for controlling the top-gate. We used a separate voltage source to power the UV LEDs. These light sources were not strictly monochromatic and have a spread in wavelength of ≈8–10 nm about the mean value. The LEDs were calibrated using a power-meter, and the wavelength of each LED was characterized by a UV–Vis spectrometer.

C. Data fitting method

Schottky barrier height (ϕ) was determined by fitting source–drain current–voltage ($I_D - V_{DS}$) curves using the modified Richardson–Dushman equation.[26–28] The back-to-back Schottky diode model offers a practical way to replicate the $I_D - V_{DS}$ behavior of FETs with source and drain contacts that form Schottky barriers with the semiconductor layer. This approach accounts for contact effects and barrier asymmetries at each contact, which is crucial for accurately depicting the current flow through the device. This model considers two Schottky diodes with barriers (ϕ_1 and ϕ_2) at the MS interface connected by a sheet resistance (R_s) shown in the inset of Fig. 1(d). The bottom contacts usually contribute to less than 100 Ω and are significantly smaller than the R_s. Hence, it was ignored for our calculations. The fitting equation is

$$I = I_0\left(\exp\left(\frac{qV'}{\eta kT}\right) - 1\right) \cdot \frac{\exp\left(\frac{-q(\phi_1+\phi_2)}{kT}\right)}{\exp\left(\frac{-q\phi_2}{kT}\right) + \exp\left(\frac{-q\phi_1}{kT} + \frac{qV'}{\eta kT}\right)}, \quad (1)$$

where $I_0 = WA^*_{2D}T^{3/2}$, η is the ideality factor of the diode, W is the contact width, $V' = V_{DS} - I_D R_S$ (R_S is the series resistance), and A^*_{2D} is the 2D Richardson constant,[29] given by

$$A^*_{2D} = \frac{q(8\pi k_B^3 m^*)^{1/2}}{h^2}. \quad (2)$$

We use the value $A^*_{2D} = 2.6 \times 10^{-4}$ A/cm $K^{3/2}$ for our analysis.

Field-effect mobility (μ) of the FET was calculated using the following relation:

$$\mu = \frac{L}{(W \cdot C \cdot V_{DS})} \times \frac{dI_D}{dV_G}, \quad (3)$$

where L and W are the length and width of the FET, respectively, C is the capacitance, I_D is the source–drain current, and V_{TG} is the top-gate voltage. Subthreshold swing is calculated using the formula $SS = \frac{dV_G}{d(\log_{10} I_D)}$, which was also monitored as a function of photodoping.

18 November 2025 09:30:49

© Author(s) 2025

III. RESULTS

Figures 1(d) and 1(e) show the room temperature current–voltage ($I_D - V_{DS}$) characteristics and the transfer characteristics ($I_D - V_{TG}$) in the pristine or dark condition. The gate leakage current is less than 0.05 nA [see supplementary material Fig. S6(a)]. We calculate the current ON/OFF ratio (I_{ON}/I_{OFF}) ≈ 10^5, SS ≈ 210 mV/dec, and μ ≈ 0.71 cm^2/Vs in this condition. The $I_D - V_{DS}$ characteristics were fit to the Richardson–Dushman equation (as described in methods), from which we extract the SB ≈ 207 meV. There is some asymmetry in $I_D - V_{DS}$ in the forward and reverse biases, because of dissimilar contact resistances between the two contacts and has been discussed in the Outlook.

Thereafter, we performed the UV irradiation experiment by exposing the hBN–MoS_2 heterostructure to UV light pulses. During the exposure, we keep V_{DS} = 1.5 V and V_{TG} = 0 V. The SiO_2/Si^{++} back-gate was not used and not grounded in the experiments and therefore can be considered to be floating in all cases.

Figure 2(a) shows current vs time ($I_D - Time$) at λ = 265 nm for three successive pulses. We observe that the current increases gradually with each UV pulse [yellow shaded portion in Fig. 2(a)], and then slightly decays when the illumination is turned off. This indicates an accumulation of electrons in MoS_2 due to photo-induced UV doping as we expected. In Fig. 2(b), we plot $I_D - V_{DS}$ in semilog as a function of decreasing wavelength of UV exposure. Figure 2(c) shows the improvement in transfer characteristics (in semilog) after exposure to decreasing wavelengths of UV light (inset shows the same in linear scale). I_D–V_{DS} and transfer characteristics were recorded after saturation is reached for each UV wavelength.

A substantial and progressive improvement of I_D happens with increasing UV exposure time. Progressively changing I_D–V_{DS} characteristics for λ = 265 nm at different exposure times is shown in Fig. 2(d). Transfer characteristics of the hBN/MoS_2 FET with increasing 265 nm UV exposure time is shown in Fig. 2(e) (the inset shows the same in linear scale). For transfer characteristics, in each case, there is enhancement in the ON-state current (I_{ON}), while the OFF-state current (I_{OFF}) remains unchanged. This is the main reason why various FET parameters drastically improve by this UV doping procedure. The corresponding gate leakage current graphs can be found in the supplementary material [Figs. S6(b) and S6(c)].

I_{ON} depends on both the wavelength and duration of UV exposure. For each UV wavelength, the current increases progressively and eventually reaches a saturation point. This saturation occurs when all available states near the band edge of the hBN layer that correspond to the energy of the incident photons have been excited and hence depleted. UV exposure beyond this point/time does not lead to any additional doping. Figure 2(f) illustrates this behavior: I_{ON} initially increases with 275 nm UV exposure, then saturates,

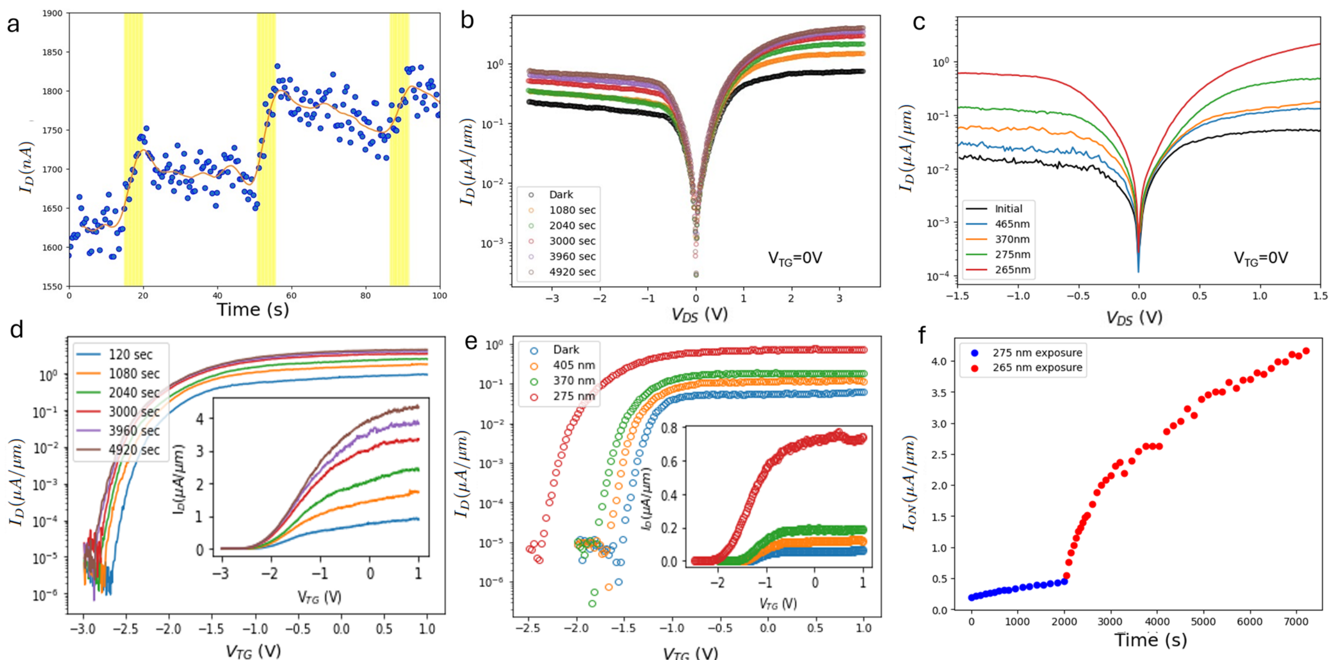

FIG. 2. Effect of UV radiation on the FET. (a) Current vs time with UV illumination at 265 nm in pulses of 10 s, with a wait time of 30 s at V_{DS} = 1.5 V. (b) $I_D - V_{DS}$ characteristics in the semi-log scale after saturation as a function of UV radiations of λ = 465, 370, 275, and 265 nm. (c) Transfer characteristics in semi-log ($I_D - V_{TG}$) at V_{DS} = 1.5 V after exposure to UV until saturation is achieved as a function of UV radiations of λ = 465, 370, and 275 nm. The inset shows transfer characteristics in linear scale. (d) $I_D - V_{DS}$ characteristics in the semi-log scale after UV illumination of 265 nm as a function of time of UV exposure. (e) Transfer characteristics in semi-log ($I_D - V_{TG}$) at V_{DS} = 1.5 V after UV illumination of 265 nm as a function of time of UV exposure. The inset shows transfer characteristics in linear scale. (f) ON-current (I_{ON}) at V_{DS} = 3.5 V and V_{TG} = 0 V with UV exposure of λ = 275 and 265 nm used in succession.

18 November 2025 09:30:49

© Author(s) 2025

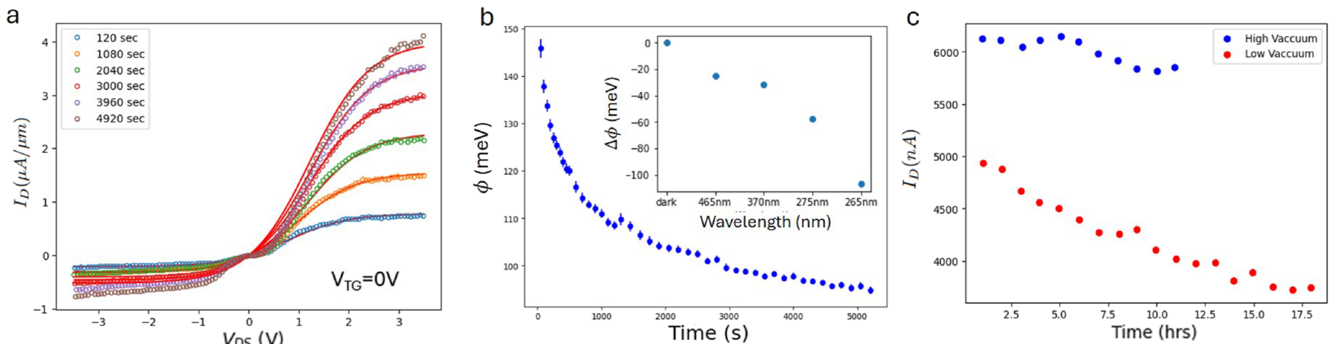

FIG. 3. Data fitting and persistence. (a) Representative $I_D - V_{DS}$ curves with the solid lines showing the fit to the experimental data, as a function of illumination exposure time t = 120, 1080, 2040, 3000, 3960, and 4920 s. (b) Schottky barrier (ϕ) as a function of UV exposure time for λ = 265 nm. Inset: The total reduction in the barrier height ($\Delta\phi$) as a function of wavelength (λ) of UV irradiation. (c) I_D as a function of time (at V_{TG} = 0 V) after UV exposure in high vacuum and low vacuum conditions.

but after switching to a 265 nm UV irradiation, which has slightly higher photon energy, I_{ON} increases further, but eventually tends toward saturation. This photodoping effect accumulates gradually with prolonged UV exposure.

At regular intervals, while applying UV pulses, $I_D - V_{DS}$ characteristics were recorded at V_{TG} = 0 V [also shown in Fig. 2(d)] and fitted using the modified Richardson–Dushman equation to extract the SB. Figure 3(a) shows $I_D - V_{DS}$ curves (shown as circles) after multiple UV exposures of λ = 265 nm, fit to the model (solid lines). The fits provide the essential parameters: ϕ_1 and ϕ_2—the Schottky barrier heights at the source and drain, respectively. The goodness of the fits has been quantified in supplementary material Sec. S5, and the normalized root-mean-square error (nRMSE) is within 1.8%–4%. The SB (ϕ) shows a gradual decrease with increasing the UV exposure [Fig. 3(b)]. Using 265 nm exposure alone, the lowered barrier height of ~148 meV is reduced to 97 meV and the ON-state current in forward bias reaches 4.2 μA/μm. The maximum reduction is observed during 265 nm exposure, owing to the large number of defect states close to E_v maxima in hBN [see Fig. 1(a)]. By n-doping the contact region, the energy mismatch between the respective Fermi levels of Au and MoS_2 is lowered, which manifests as a reduction in the SB. The inset of Fig. 3(b) shows the total decrease in SB as a function of wavelength of irradiation. Persistence effect of photodoping is shown by Fig. 3(c). It shows the decay of the increased ON-state current over a prolonged period in high and low vacuum conditions. Reduced SB leads to decreased contact resistance and improved carrier injection efficiency, which leads to improved FET performance. The gradual performance improvement due to 265 nm exposure is quantified using various FET parameters, such as I_{ON}/I_{OFF}, mobility, and subthreshold swing in Fig. 4.

IV. DISCUSSIONS

A. Persistence of the photodoping

In Fig. 2(a), we observe that I_D slightly decays when the UV pulse is off. Although the enhanced ON-state current does decay over time, the decay is relatively slow and the photodoping effect is not transient. As seen in Fig. 3(c), the decay rate is very less in high vacuum condition (10^{-6} mbar) and slightly more in low vacuum condition (10^{-3} mbar). This suggests that there may be two mechanisms that are responsible for this slight decay in current:

1. Electron tunneling from the MoS_2 layer back to the positively charged hBN defect sites, partially neutralizing the doping effect.
2. Charge compensation by ambient dipolar molecules, which may donate electrons to the charged hBN and reduce its net positive charge.

18 November 2025 09:30:49

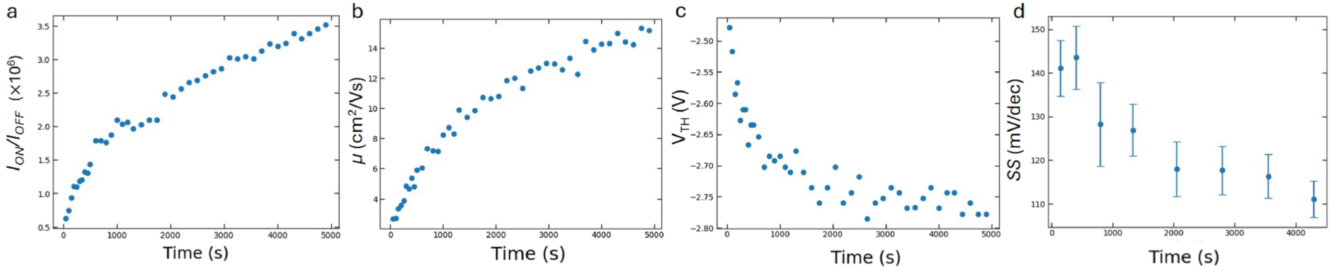

FIG. 4. Progressive improvement in device parameters upon UV illumination at λ = 265 nm with exposure time at V_{DS} = 3.5 V. (a) ON–OFF ratio (I_{ON}/I_{OFF}) (b) Mobility (μ). (c) Threshold voltage (V_{TH}). (d) Subthreshold Swing (SS) with exposure time.

© Author(s) 2025

B. Effect of UV wavelengths on hBN defects

In Fig. 2(f), we observe that I_D saturates to a value after prolonged UV exposure, but after lowering the wavelength of the UV radiation, there is again a rise in I_D. This maybe explained by the defect states in hBN. Figure 1(a) shows the various defect states present in hBN.[30] These defect states arise from native vacancies, anti-sites, and impurity centers—particularly substitutional carbon (C_B, C_N), oxygen (O_N), and hydrogen-related complexes, such as V_B-3H.[31,32] Several of these exhibit deep donor levels near midgap and closer to the valence band maximum (VBM), with $0/1^+$, $1^+/2^+$, or $1^-/0$ charge transition levels. This energy range corresponds to photon energies between ~2.5–4.5 eV, or wavelengths of 495–275 nm. Hence, the choice of UV LEDs (e.g., 405, 365, 307, and 265 nm). For instance, the $0/1^+$ transition of the C_B defect occurs at 3.71 eV (334 nm), while V_B-H and V_B-2H transitions lie at 4.34–4.45 eV (corresponding to ~285–275 nm), placing them within the absorption range of our deep UV illumination. Upon photoexcitation, electrons from these donor-like defect levels are promoted to the conduction band of hBN and may subsequently tunnel into the adjacent MoS_2 layer, whose conduction band minimum lies at ~4.2 eV below vacuum. Since the MoS_2 layer is electrically grounded during illumination, the photo-excited electrons are rapidly drained, leaving behind local positive charge sites in hBN, as discussed previously. The energy level of these defects lie below the Fermi level of hBN and are hence very stable.

C. Exposure dependence of device parameters

Key device performance parameters were monitored as the UV doping process continued. Upon successive exposure to other wavelengths before using 265 nm, the I_{ON}/I_{OFF} is increased by six times Fig. 4(a). The mobility increased from the pristine value of ≈0.71 to ≈2.4 cm^2/Vs, and upon illumination of 265 nm UV light, it improved from ≈2.4 to ≈15.1 cm^2/Vs [see Fig. 4(b)]. While local top-gate protects the channel region, a fraction of UV intensity probably delocalizes some electrons, putting them into the conduction band. Note that it will not change the threshold voltage [(V_{TH}, shown in Fig. 4(c)] appreciably. However, these delocalized electrons provide more efficient screening of the disorder potential, leading to an improved mobility. Thus, our analysis indicates improved carrier injection at the metal–semiconductor junction and reduced contact resistance, due to lowering of the SB [see Fig. 3(b)]. In Fig. 4(c), we plot V_{TH} as a function of UV exposure. We observe that V_{TH} shifts by about −0.3 V, suggesting only a minimal doping of the channel region. Even though the MoS_2 channel is shielded by the top gate electrode (50 nm Au), ~0.2%[33] of the incident UV light (in range 400–265 nm) penetrates through the metal gate. This causes the hBN covering the channel to develop stored charges, which leads to doping of the channel. The carrier density induced (with UV irradiation at 265 nm) in the channel is estimated to be $\Delta n \approx 2.9 \times 10^{11}$ cm^{-2}, while near the contacts, it is estimated to be $\Delta n \approx 2.4 \times 10^{12}$ cm^{-2}. Hence, the contact regions are doped nearly an order of magnitude more than the channel region (see supplementary material Sec. S7). The direct absorption of UV light by monolayer MoS_2 is weak and the UV-induced excitation within MoS_2 is negligible. Its contribution to the overall doping process is significantly smaller compared to the excitation and tunneling from the hBN layer. Figure 4(d) shows a decrease of the *SS* from 148 to 90 mV/dec, indicating that the FET channel characteristics have improved.

D. SB engineering with diverse 2D semiconductors

We tested the photodoping strategy with UV irradiation on devices fabricated with other 2D layered semiconductors, such as $MoSe_2$ and WSe_2, along with MoS_2. Experimental data with UV exposure are given in the supplementary material, Sec. S3. We observe that in both cases, there is a substantial increase in the ON-state current, while the OFF-state current remains unchanged. The reduction in SB for $MoSe_2$ was from 120 to 96 meV, while for WSe_2, it was from 235 to 198 meV. In Figs. 5(a) and 5(b), we show the comparative reduction in SB (and increase in mobility) for all three different TMD-based FETs. In all cases, there is a substantial decrease in the SB with UV exposure, Though, in the case of MoS_2, the change is maximum. The efficiency of this charge transfer process is primarily governed by the difference in energy levels between the conduction band of TMD and the excited defect states in hBN. Since the tunneling electrons transition from hBN into TMD, this conduction band alignment is critical.

In Fig. 5(c), we compare the energy levels of the various components of the FET: Au, hBN, and TMDs. The variations in the doping process for different TMDs can be attributed to intrinsic differences in conduction band alignment and dielectric screening.

18 November 2025 09:30:49

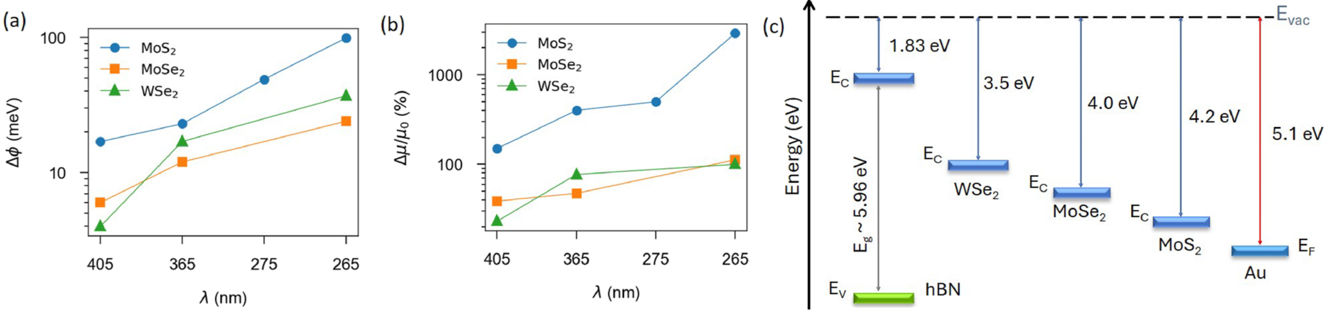

FIG. 5. Comparison of UV radiation on diverse TMD-based FETs. (a) $\Delta\phi$ as a function of wavelength in MoS_2, $MoSe_2$, and WSe_2. (b) $\Delta\mu/\mu$ in % as a function of wavelength in MoS_2, $MoSe_2$, and WSe_2. (c) Representative schematic of the energy levels in different monolayer TMDs[34,35] in comparison to Au and hBN.

© Author(s) 2025

Electron affinity varies across the materials and their thicknesses, increasing from 3.6 to 3.9 eV for WSe_2 and 3.8–4.1 eV for $MoSe_2$, up to 4.2–4.3 eV for MoS_2.[34,35] This indicates that the doping efficiency can be tuned by material choice and their thickness. The work function of the metal does not directly influence the optically induced charge transfer process, although it may indirectly affect it via contact-induced doping, which in turn alters its band alignment.

E. Outlook: UV-induced photodoping process

The UV-induced photodoping addresses several limitations of conventional doping:

1. *Channel preservation*: UV light is absorbed by the top metal gate, shielding the channel region from exposure and preserving its intrinsic properties. In contrast, many previous photodoping methods exposed the entire device to illumination, often leading to excessive channel doping while leaving the contacts relatively unaffected.
2. *Damage-free processing*: The process is entirely optical, avoiding the chemical steps that may damage the TMD. The UV light used in the experiment has energy <4.6 eV, which minimizes the risk of lattice degradation.
3. *High spatial resolution control*: The spatial resolution of our UV doping technique depends on the spot size of the beam and the hBN thickness. It contributes to the doping region due to fringing electric fields from the charges stored within it. For example, for a 20 nm thick hBN layer, the final doping resolution is approximately the beam spot size plus a broadening factor on the order of the hBN thickness.

While the photodoping strategy is effective, our device architecture presents certain drawbacks. The TMD layer is stamped onto metal contacts, which possess inherent surface roughness.[36] The TMD wraps around the bottom contacts, which causes some strain to develop, which can also cause n−doping. This leads to non-uniform contact interfaces and hence unequal contact resistance. As a result, the initial device performance is limited, with $I_{ON} \approx 50$ nA/μm in forward bias and 15 nA/μm in reverse bias [see Fig. 1(d)], reflected in the asymmetry in the SB as well. This is also the reason why the transmission line method could not be used to extract the contact resistance. The effectiveness of photodoping in the hBN/TMD heterostructures is strongly influenced by the thickness of both the hBN and TMD layers. The photodoping effect is not strictly a bulk phenomenon for hBN. Prior work has shown that few-layer hBN can host optically active defect states capable of charge trapping.[30] Thicker hBN layer (≈20 nm) has deeper defect states and higher defect density, which can provide greater capacity for charge retention, potentially enhancing the doping strength and stability observed in our devices.[37] In contrast, thicker TMD layers exhibit higher out-of-plane dielectric constants, which lead to stronger electrostatic screening of the electric field generated by charged hBN defects. This reduces the modulation of the TMD Fermi level and limits the reduction in the Schottky barrier height. Thus, thinner TMD layers are more responsive to photodoping, while moderately thick hBN (≈20 nm) layers provide a more effective platform for charge retention and doping persistence. Optimizing the relative thickness of both layers is therefore critical for maximizing the photodoping efficiency in these heterostructures. The photodoping effect remains notably stable over several days in high vacuum conditions [see Fig. 2(e)]. However, its gradual decay under atmospheric exposure suggests a sensitivity to environmental factors, such as adsorbed dipolar molecules. This behavior implies potential for reversible doping control under vacuum or inert environments, opening avenues for re-writable device applications as well.

V. CONCLUSION

In this work, we establish a novel UV-induced photodoping strategy to selectively dope the contacts of a TMD/Au junction, quantified by the reduction in the SB by ≈100 meV and enhancement in the ON-state current by seventy times in a MoS_2/hBN FET. Mobility is improved from 0.71 cm^2/Vs in the initial dark state to 15.1 cm^2/Vs in the final state after UV exposure. Using 265 nm UV irradiation alone, the mobility and I_{ON}/I_{OFF} ratio are increased by six times, and the subthreshold swing decreased by 1.3 times, highlighting the effectiveness of UV-induced photodoping as a strategy to improve the performance of TMD-based FETs. Unlike chemical doping, this method introduces no structural damage, enables spatially selective doping, and avoids channel contamination by leveraging the optical absorption properties of hBN. The strategy was verified for different TMDs (exhibiting varying SB) and showed a significant reduction in the SB and improved device characteristics, establishing that the strategy employed here is universal and applicable for other semiconductors as well. This photodoping approach is reversible, broadly applicable, and compatible with post-fabrication processing, making it a versatile contact engineering technique for next-generation 2D electronics. With further optimization of UV protocols and device geometry, this method could support scalable, high-performance transistor technologies requiring localized or reconfigurable doping.

SUPPLEMENTARY MATERIAL

The supplementary material includes device fabrication and characterization, experimental data on other TMD/hBN FETs, calculations on charge-doping by UV radiation, errors due to fitting, and estimate of channel doping due to UV illumination.

ACKNOWLEDGMENTS

The authors acknowledge the usage of NNFC facilities at CeNSE, IISc and funding from the Department of Science and Technology (DST), Government of India. A.G. acknowledges the J. C. Bose Fellowship (Grant No. SP/DSTO-18-2038) from the Science and Engineering Research Board, DST, and Nano Mission, DST, Government of India, for financial support under Grant No. DST/NM/TUE/QM-10/2019. S.S. acknowledges financial support from the University Grants Commission (Grant No. IE-REAC-23-0168). K.W. and T.T. acknowledge support from the JSPS KAKENHI (Grant Nos. 21H05233 and 23H02052), the CREST (Grant No. JPMJCR24A5), JST, and World Premier International Research Center Initiative (WPI), MEXT, Japan.

18 November 2025 09:30:49

© Author(s) 2025

AUTHOR DECLARATIONS

Conflict of Interest

The authors have no conflicts to disclose.

Author Contributions

Somaditya Santra and Shaili Sett contributed equally to this paper.

S. Santra, S. Samdariya, and S. Sett fabricated the devices. S. Santra and S. Sett performed the measurements, analyzed the data, and wrote the manuscript. S. Samdariya supported with measurements and analysis. K.W. and T.T. grew the hBN crystals. A.G. supervised the overall project, edited, and revised the manuscript.

Somaditya Santra: Data curation (lead); Formal analysis (lead); Investigation (equal); Methodology (equal); Validation (equal); Writing – original draft (equal). **Sankalp Samdariya**: Investigation (supporting); Methodology (supporting). **Shaili Sett**: Data curation (supporting); Formal analysis (supporting); Investigation (equal); Methodology (equal); Supervision (supporting); Writing – original draft (equal); Writing – review & editing (equal). **Kenji Watanabe**: Resources (supporting). **Takashi Taniguchi**: Resources (supporting). **Arindam Ghosh**: Conceptualization (lead); Funding acquisition (lead); Project administration (equal); Supervision (equal); Writing – review & editing (equal).

DATA AVAILABILITY

The data that support the findings of this study are available from the corresponding author upon reasonable request.

REFERENCES

[1] Y. Wang, S. Sarkar, H. Yan, and M. Chhowalla, "Critical challenges in the development of electronics based on two-dimensional transition metal dichalcogenides," Nat. Electron. **7**, 638 (2024).
[2] Y. Liu, X. Duan, H.-J. Shin, S. Park, Y. Huang, and X. Duan, "Promises and prospects of two-dimensional transistors," Nature **591**, 43 (2021).
[3] Y. Wang, J. C. Kim, R. J. Wu, J. Martinez, X. Song, J. Yang, F. Zhao, A. Mkhoyan, H. Y. Jeong, and M. Chhowalla, "Van der Waals contacts between three-dimensional metals and two-dimensional semiconductors," Nature **568**, 70 (2019).
[4] Y. Wang, J. C. Kim, Y. Li, K. Y. Ma, S. Hong, M. Kim, H. S. Shin, H. Y. Jeong, and M. Chhowalla, "P-type electrical contacts for 2D transition-metal dichalcogenides," Nature **610**, 61 (2022).
[5] W. Liu, J. Kang, D. Sarkar, Y. Khatami, D. Jena, and K. Banerjee, "Role of metal contacts in designing high-performance monolayer n-type WSe_2 field effect transistors," Nano Lett. **13**, 1983 (2013).
[6] Y. Jung, M. S. Choi, A. Nipane, A. Borah, B. Kim, A. Zangiabadi, T. Taniguchi, K. Watanabe, W. J. Yoo, J. Hone, and J. T. Teherani, "Transferred via contacts as a platform for ideal two-dimensional transistors," Nat. Electron. **2**, 187 (2019).
[7] A. Allain, J. Kang, K. Banerjee, and A. Kis, "Electrical contacts to two-dimensional semiconductors," Nat. Mater. **14**, 1195 (2015).
[8] V. Heine, "Theory of surface states," Phys. Rev. **138**, A1689 (1965).
[9] J. Kumar and M. Shrivastava, "Role of chalcogen defect introducing metal-induced gap states and its implications for metal–TMDs' interface chemistry," ACS Omega **8**, 10176 (2023).
[10] P.-C. Shen, C. Su, Y. Lin, A.-S. Chou, C.-C. Cheng, J.-H. Park, M.-H. Chiu, A.-Y. Lu, H.-L. Tang, M. M. Tavakoli, G. Pitner, X. Ji, Z. Cai, N. Mao, J. Wang, V. Tung, J. Li, J. Bokor, A. Zettl, C.-I. Wu, T. Palacios, L.-J. Li, and J. Kong, "Ultralow contact resistance between semimetal and monolayer semiconductors," Nature **593**, 211 (2021).
[11] W. Li, X. Gong, Z. Yu, L. Ma, W. Sun, S. Gao, Ç. Köroğlu, W. Wang, L. Liu, T. Li, H. Ning, D. Fan, Y. Xu, X. Tu, T. Xu, L. Sun, W. Wang, J. Lu, Z. Ni, J. Li, X. Duan, P. Wang, Y. Nie, H. Qiu, Y. Shi, E. Pop, J. Wang, and X. Wang, "Approaching the quantum limit in two-dimensional semiconductor contacts," Nature **613**, 274 (2023).
[12] R. Nakajima, T. Nishimura, K. Ueno, and K. Nagashio, "Work function modulation of Bi/Au bilayer system toward p-type WSe_2 FET," ACS Appl. Electron. Mater. **6**, 144 (2023).
[13] T. Su, Y. Li, Q. Wang, W. Zhao, L. Cao, and Y. S. Ang, "Semimetal contacts to monolayer semiconductor: Weak metalization as an effective mechanism to Schottky barrier lowering," J. Phys. D: Appl. Phys. **56**, 234001 (2023).
[14] G.-S. Kim, S.-W. Kim, S.-H. Kim, J. Park, Y. Seo, B. J. Cho, C. Shin, J. H. Shim, and H.-Y. Yu, "Effective Schottky barrier height lowering of metal/n-Ge with a TiO_2/GeO_2 interlayer stack," ACS Appl. Mater. Interfaces **8**, 35419 (2016).
[15] H.-J. Chuang, B. Chamlagain, M. Koehler, M. M. Perera, J. Yan, D. Mandrus, D. Tománek, and Z. Zhou, "Low-resistance 2D/2D ohmic contacts: A universal approach to high-performance WSe_2, MoS_2, and $MoSe_2$ transistors," Nano Lett. **16**, 1896 (2016).
[16] C. J. McClellan, E. Yalon, K. K. H. Smithe, S. V. Suryavanshi, and E. Pop, "High current density in monolayer MoS_2 doped by AlO_x," ACS Nano **15**, 1587 (2021).
[17] R. Kappera, D. Voiry, S. E. Yalcin, B. Branch, G. Gupta, A. D. Mohite, and M. Chhowalla, "Phase-engineered low-resistance contacts for ultrathin MoS_2 transistors," Nat. Mater. **13**, 1128 (2014).
[18] L. Tang, R. Xu, J. Tan, Y. Luo, J. Zou, Z. Zhang, R. Zhang, Y. Zhao, J. Lin, X. Zou, B. Liu, and H.-M. Cheng, "Modulating electronic structure of monolayer transition metal dichalcogenides by substitutional Nb-doping," Adv. Funct. Mater. **31**, 2006941 (2021).
[19] L. Ju, J. Velasco, E. Huang, S. Kahn, C. Nosiglia, H.-Z. Tsai, W. Yang, T. Taniguchi, K. Watanabe, Y. Zhang, G. Zhang, M. Crommie, A. Zettl, and F. Wang, "Photoinduced doping in heterostructures of graphene and boron nitride," Nat. Nanotechnol. **9**, 348 (2014).
[20] M. A. Khan, M. F. Khan, S. Rehman, H. Patil, G. Dastgeer, B. M. Ko, and J. Eom, "The non-volatile electrostatic doping effect in $MoTe_2$ field-effect transistors controlled by hexagonal boron nitride and a metal gate," Sci. Rep. **12**, 12085 (2022).
[21] J. Quereda, T. S. Ghiasi, C. H. van der Wal, and B. J. van Wees, "Semiconductor channel-mediated photodoping in h-BN encapsulated monolayer $MoSe_2$ phototransistors," 2D Mater. **6**, 025040 (2019).
[22] X. Luo, K. Andrews, T. Wang, A. Bowman, Z. Zhou, and Y.-Q. Xu, "Reversible photo-induced doping in WSe_2 field effect transistors," Nanoscale **11**, 7358 (2019).
[23] A. C. Gadelha, A. R. Cadore, L. Lafeta, A. M. de Paula, L. M. Malard, R. G. Lacerda, and L. C. Campos, "Local photodoping in monolayer MoS_2," Nanotechnology **31**, 255701 (2020).
[24] R. Zhang, Z. Xie, C. An, S. Fan, Q. Zhang, S. Wu, L. Xu, X. Hu, D. Zhang, D. Sun, J.-H. Chen, and J. Liu, "Ultraviolet light-induced persistent and degenerated doping in MoS_2 for potential photocontrollable electronics applications," ACS Appl. Mater. Interfaces **10**, 27840 (2018).
[25] C. D. English, G. Shine, V. E. Dorgan, K. C. Saraswat, and E. Pop, "Improved contacts to MoS_2 transistors by ultra-high vacuum metal deposition," Nano Lett. **16**, 3824 (2016).
[26] H. Norde, "A modified forward I-V plot for Schottky diodes with high series resistance," J. Appl. Phys. **50**, 5052 (1979).
[27] S. Sett, K. Das, and A. K. Raychaudhuri, "Investigation of factors affecting electrical contacts on single germanium nanowires," J. Appl. Phys. **121**, 124503 (2017).
[28] Y. S. Ang, L. Cao, and L. K. Ang, "Physics of electron emission and injection in two-dimensional materials: Theory and simulation," InfoMat **3**, 502 (2021).
[29] A. Anwar, B. Nabet, J. Culp, and F. Castro, "Effects of electron confinement on thermionic emission current in a modulation doped heterostructure," J. Appl. Phys. **85**, 2663 (1999).

18 November 2025 09:30:49

© Author(s) 2025

[30] L. Weston, D. Wickramaratne, M. Mackoit, A. Alkauskas, and C. G. Van de Walle, "Native point defects and impurities in hexagonal boron nitride," Phys. Rev. B **97**, 214104 (2018).
[31] P. Pal, S. Bhowmik, A. Parappurath, S. Kakkar, K. Watanabe, T. Taniguchi, and A. Ghosh, "Low-frequency resistance noise in near-magic-angle twisted bilayer graphene," ACS Nano **19**, 3240 (2025).
[32] J. R. Reimers, J. Shen, M. Kianinia, C. Bradac, I. Aharonovich, M. J. Ford, and P. Piecuch, "Photoluminescence, photophysics, and photochemistry of the V_B^- defect in hexagonal boron nitride," Phys. Rev. B **102**, 144105 (2020).
[33] P. B. Johnson and R. W. Christy, "Optical constants of the noble metals," Phys. Rev. B **6**, 4370 (1972).
[34] J. Xiao, Y. Zhang, H. Chen, N. Xu, and S. Deng, "Enhanced performance of a monolayer MoS_2/WSe_2 heterojunction as a photoelectrochemical cathode," Nano-Micro Lett. **10**, 60 (2018).
[35] Q. Zhang, S. Zhang, B. A. Sperling, and N. V. Nguyen, "Band offset and electron affinity of monolayer $MoSe_2$ by internal photoemission," J. Electron. Mater. **48**, 6446 (2019).
[36] S. Banerjee, L. Cao, Y. S. Ang, L. K. Ang, and P. Zhang, "Reducing contact resistance in two-dimensional-material-based electrical contacts by roughness engineering," Phys. Rev. Appl. **13**, 064021 (2020).
[37] D. Wang and R. Sundararaman, "Layer dependence of defect charge transition levels in two-dimensional materials," Phys. Rev. B **101**, 054103 (2020).

18 November 2025 09:30:49

© Author(s) 2025